Electronic structure and bonding in the Y-Si-O-N quaternary crystals

W. Y. Ching,* Lizhi Ouyang, Hongzhi Yao, and Yong Nian Xu
Department of Physics, University of Missouri-Kansas City, Kansas City, Missouri 64110, USA
(Received 12 February 2004; published 10 August 2004)

The Y-Si-O-N quaternary crystals are an important part of structural ceramics. Their crystal structures are complex and not precisely determined. Little is known about their electronic structure and bonding which are indispensable for a fundamental understanding of structural ceramics. Within the equilibrium phase diagram of the SiO_2-Y_2O_3-Si_3N_4 system, there are only four known crystalline phases: $Y_2Si_3N_4O_3$ (M-melilite), $Y_4Si_2O_7N_2$ (*J* phase or N-YAM), $YSiO_2N$ (wallastonite), and $Y_{10}[SiO_4]_6N_2$ (N-apatite). With the possible exception of $YSiO_2N$, these crystals have O/N disorder in that the exact positions of the anions cannot be uniquely determined. Using accurate *ab initio* total energy relaxation, the atomic positions of the lowest energy configurations in these crystals are determined. Based on the theoretically modeled structures, the electronic structure and bonding are investigated using the *ab initio* orthogonalized linear combination of atomic orbitals method, and are related to a variety of local cation-anion bonding configurations. These results are presented in the form of atom-resolved partial density of states, Mulliken effective charges and bond order values. Although the strong Si-N and Si-O bonding dominates in these crystals, it is also shown that Y-O and Y-N bonding are not negligible and should be a part of discussion of the overall bonding scheme in these crystals. It is concluded that $Y_2Si_3N_4O_3$ has the strongest crystal bonding among the four crystals. In addition, the optical properties of these crystals are calculated using the *ab initio* wave functions. All four crystals are insulators with optical band gaps of 3.40, 3.19, 4.40, and 3.70 eV, respectively. These results are further discussed in the context of specific bonding configurations of the cations (Si and Y) with the anions (O and N) and their implications on the metal-containing intergranular glassy films in polycrystalline Si_3N_4.

DOI: 10.1103/PhysRevB.70.085105 PACS number(s): 71.20.Ps, 78.40.Ha

I. INTRODUCTION

Nitrogen ceramics always play an important role in structural ceramics with applications in cutting tools, engine components, and microelectronics.[1] The outstanding properties of Si_3N_4 in thermal stability, resistance to corrosion and thermal shocks, chemical durability and higher dielectric constant are well known. To extend their range of application, quaternary systems such as Si-Al-ON have been actively investigated[2–4] since its discovery in the early 1970s.[5,6] In the Si-Al-ON system, a (Si,N) pair is replaced by a (Al,O) pair to preserve charge neutrality and electronic structure calculation shows very little modification in charge redistribution.[7] On the other hand, the quaternary system of Y-Si-O-N is much less studied. Although both Y and Al are considered to have formal valence of 3+, Y is a much larger ion and its bonding to O and N anions is far more complicated. They are only four confirmed crystalline phases of Y-Si-O-N compounds[8–10] at the interior of the SiO_2-Y_2O_3-Si_3N_4 phase equilibrium diagram shown in Fig. 1. They are $Y_2Si_3N_4O_3$ (M-melilite), $Y_4Si_2O_7N_2$ (*J* phase or N-YAM), $YSiO_2N$ (wallastonite), and $Y_{10}[SiO_4]_6N_2$ (N-apatite) (see Fig. 2). They occur mostly as secondary phases in the hot-pressed sintering of polycrystalline Si_3N_4 and SiAlON using Y_2O_3 as the sintering aid for densification.[1,10] Little is known about the structures and properties of these complex crystals. For the structures, only the space group and the approximate lattice constants were reported by several groups and they usually differ considerably.[8,10–14] Most of the past studies on these quaternary crystals concentrate on the processing conditions or their role as undesirable precipitated phases.[15,16] The lack of single crystals and pure single-phase samples contributed to the structural uncertainty of these compounds. Furthermore, it is quite well known that O/N disorder exists in these crystals and x-ray diffraction experiment can hardly distinguish between O and N. Without the knowledge of the exact atomic positions, no reliable electronic structure calculations can be performed. As a result, detailed information on the electronic structure and bonding in these crystals is not available. In contrast, the electronic structures of the Si-Al-O-N system have been reported by several groups recently.[7,17–19]

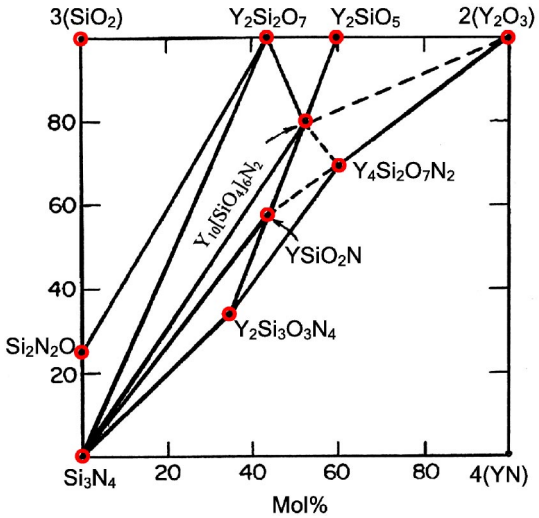

FIG. 1. The SiO_2-Y_2O_3-Si_3N_4 phase diagram.

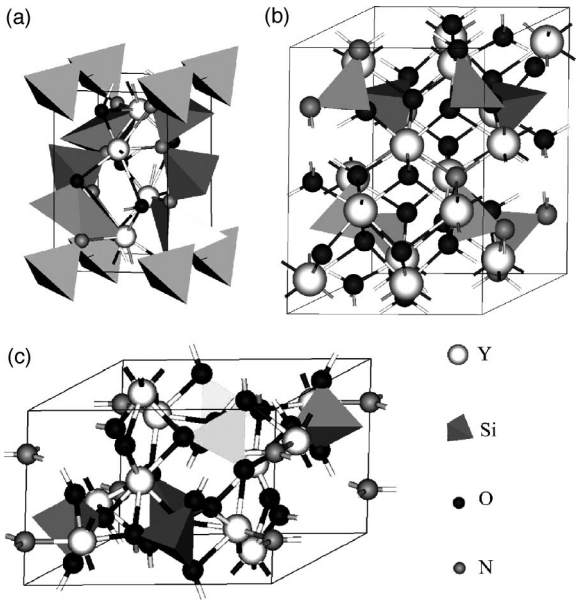

FIG. 2. Sketch of the crystals structures of: (a) $Y_2Si_3N_4O_3$, (b) $Y_4Si_2O_7N_2$, and (c) $Y_{10}[SiO_4]_6N_2$ without O/N disorder.

Most research in N-ceramics concentrates on processing condition and phase identification, with little attention to the fundamental aspects of these materials and their physical properties. In this paper, we present the results of a comprehensive investigation of the electronic structure and bonding of the four quaternary Y-Si-O-N crystals. A plethora of cation-anion bonding configurations in these crystals provide the important insight on the structural aspects of the materials with implications to Y-Si-O-N glasses.[20] Detailed electronic structure calculation can also shed much light on possible local Si-O and Si-N bonding which has been subjected to several experimental investigations using $^{29+}$Si nuclear magnetic resonance (NMR) with magic angle spinning technique.[21–25] The information obtained from these experiments so far is only qualitative at most. Their interpretation can be greatly facilitated by detailed theoretical calculations where the specific arrangements of Si-O and Si-N bonding are known. Y-Si-O-N crystals have also been suggested as possible photoluminescence materials that can accommodate rare earth ions such as Ce^{3+} for possible electro-optical applications.[26] The stoke shifts observed in different host crystals with different N content is related to the increased rigidity of the lattice. It has also been speculated that N-apatite or $Y_{10}[SiO_4]_6N_2$ could be an ideal host material for the encapsulation of nuclear waste.[27]

The main motivation for us to study the electronic structure and bonding in Y-Si-O-N quaternary crystals is to understand the structure and properties of intergranular glassy films (IGFs) in polycrystalline Si_3N_4. The existence of thin IGFs with a constant thickness of about a nanometer thick in Si_3N_4 and other ceramic polycrystals sintered at high temperature has been known for quite some time and is a very active area of ceramic research.[28–36] These IGFs control the overall mechanical properties and creep behavior at high temperature,[37–39] and hence the functionality of the devices made of them. The thickness and the microstructures of IGF and the connected glassy phase at the triple junction can be greatly affected by the presence of different metal solvents, usually rare earth ions originated from the sintering aids in the sintering process. Steric model for equilibrium thickness of IGF based on the balance of attractive van der Waal forces and repulsive steric forces had been proposed.[40] The local bonding structure and the role played by the metal ions in the formation of and the subsequent chemical equilibrium of IGFs is a subject of considerable interest and debate.[41–44] There have been some attempts to model the IGF structures using molecular dynamic simulations.[44–47] Since the local structure of IGF is totally unknown, such simulations and the resulting models depend on the initially assumed structure and the potential used in the simulation, which may or may not be consistent with the real structure of IGF. Yoshiya *et al.* found a high density of dangling bonds at the interface of such models.[46] Furthermore, such IGF models usually contain at least several thousands of atoms. No realistic electronic structure calculation using *ab initio* methods can be attempted on such models. The only *ab initio* calculation so far on the properties of IGF employs a small cluster of atoms with some plausible constraints.[48] In this respect, detailed calculation of electronic structure and bonding of the quaternary Y-Si-O-N crystals will be very worthwhile for the following reasons. First, Y represents a typical metallic ion in IGF. Such study may provide information on the atomic scale bonding of the Y ion at the near-prism plane of the interface structure in Si_3N_4.[49] Second, if the atomic positions and the local coordination of these crystals are determined, electronic structure can be calculated and correlated with their structural characteristics. Third, if all known crystalline phases in the quaternary system are studied together, a variety of different bonding configurations can be identified. It is conceivable that similar local bonding structures would be present in the real IGF structures. Lastly, the information thus obtained can provide useful input in the construction of more realistic IGF models for large-scale simulations.

Over the last several years, we have studied the electronic structure and optical properties of the binary and ternary crystals of Fig. 1. They are SiO_2 (α-quartz and amorphous SiO_2)[50,51], β-Si_3N_4[52], and Y_2O_3 (Ref. 53) as well as the ternary crystal Si_2N_2O.[52] More recently, we have also studied the other two more complex ternary compounds $Y_2Si_2O_7$ and Y_2SiO_5.[54] For quaternary crystals, we have just published the results for $YSiO_2N$ using the structure determined by *ab initio* modeling.[55]. For $Y_{10}[SiO_4]_6N_2$, we have reported a preliminary study[56] based on the ideal apatite structure in which the N atoms are assumed to be at the F site ($2a$) in fluoroapatite $Ca_{10}[PO_4]_6F_2$. The electronic structure of that calculation shows some very peculiar features in the band structure and density of states (DOS).[56] It was pointed out by Morgan[57] that this structure is highly unlikely because it violates Pauling's second crystal rule (PSCR).[58,59] The PSCR states that the valence of the anion is equal to the sum of the valence of the cations arriving at the anion divided by the coordination of that cation. The more likely structure should be the one in which N is directly bonded to Si. It is therefore quite obvious that in N-apatite, O/N disorder exists and the real structure must deviate from the perfect apatite structure. The crystal structures of the other two quaternary crystals, $Y_2Si_3N_4O_3$ and $Y_4Si_2O_7N_2$, have been reported by several

TABLE I. Measured and relaxed crystal parameters of the four quaternary crystals. The relaxed parameters are in parentheses.

Crystals	$Y_2Si_3N_4O_3^*$	$Y_4Si_2O_7N_2$	$YSiO_2N$	$Y_{10}[SiO_4]_6N_2$
Space group	$P\text{-}42_1m$ ($P2_1$)	$P2_1/c$ ($P2_1/c$)	$P6_1$ ($P6_122$)	$P63/m$ (P_{21}/m)
Space group No.	113 (4)	14 (14)	169 (178)	176 (11)
Structure	N-melilite	*J* phase, N-YAM	Wollastonite	N-apatite, H phase
Lattice constants (Å)				
a	7.6083 (7.4238)	7.5601	7.021 (6.9952)	9.6388 (9.1246)
b	(7.6027)	10.4411	⋯	(6.7302)
c	4.9113 (4.8162)	10.7626	27.3 (27.5179)	6.5609 (9.0413)
β	(89.938°)	110.042°	120° (120°)	(119.008°)
No. atoms/cell	24 $Z=2$	60 $Z=4$	90 $Z=18$	42 $Z=2$
Cell vol. (Å^3)	271.813	798.106	1165.443	485.676

groups.[8,12,13] Because of the presence of the O/N disorder, the reported O and N positions have partial occupations and the precise atomic positions are not known. In order to study the electronic structure of these two crystals, atomic positions must be determined first before any calculations can be performed. Fang *et al.* reported such a calculation for $Y_2Si_3N_4O_3$,[60] while no calculation has been done (to our best knowledge) for $Y_4Si_2O_7N_2$ mainly because of its extremely complex crystal structure.

In this paper, we use the reported crystal structure by MacKenzie *et al.*[12] and determine the exact atomic positions using a total energy minimization scheme based on *ab initio* density functional theory together with a symmetry analysis tool.[61] We then use the time-tested orthogonalized linear combination of atomic orbitals (OLCAO) method[62] to calculate and analyze the electronic structure and bonding in these three crystals. Together with the results of $YSiO_2N$,[55] the electronic structure and bonding in all four quaternary crystals are presented and compared in a comprehensive way.

The paper is organized as follows. We first describe the procedures and the results of crystal structure analysis in Sec. II. In Sec. III, we present and discuss the results of the electronic structure and bonding in these crystals. The calculated optical properties are presented and elaborated in Sec. IV. The last section is devoted to additional discussions and some conclusions, and outlines the possible directions of future work in Y-Si-O-N and related systems.

II. CRYSTAL STRUCTURES AND THE O/N DISORDER

The crystal structures of all four quaternary Y-Si-O-N crystals have never been precisely determined mainly because single crystals are impossible to obtain. Most of the measurements were done by powder diffraction on polycrystal samples that were believed to be of single phase. Lattice constants and space groups for these crystals were established from the diffraction data. It has been suggested that $Y_2Si_3N_4O_3$ has a space group of $P\text{-}42_1m$ with two formula units (f.u.) in the tetragonal unit cell and $Y_4Si_2O_7N_2$ (space group $P2_1/c$) has a monoclinic cell with 4 f.u. It is isostructural to the mineral cuspidine $Ca_4Si_2O_7F_2$ that was synthesized by Saburi *et al.*[63] $Y_4Si_2O_7N_2$ and the many other similar $RE_4Si_2O_7N_2$ (RE=rare earth) crystals are collectively known as the *J* phase. The crystal parameters of $Y_2Si_3N_4O_3$ and $Y_4Si_2O_7N_2$ based on the measurements of MacKenzie *et al.*[12] who were the only ones who did the Rietveld refinements for these crystals are listed in Table I. Although the atomic positions of these two crystals were listed in Ref. 12, the O and N sites involve partial occupations because the x-ray diffraction technique cannot distinguish O and N. Mackenzie *et al.* proposed four possible models of O/N positions in $Y_4Si_2O_7N_2$ but were unable to identify the most likely one because of the small differences in the *R* values in these refinements.[12] Of the four quaternary crystals, $YSiO_2N$ has the most complicated structure with 90 atoms in the hexagonal unit cell (18 f.u./cell). As has been discussed in considerable detail in Ref. 55, the original suggested structure for $YSiO_2N$ by Morgan *et al.*[11] is only an approximate one. Subsequent *ab initio* relaxation revealed a better description for this phase. It has a lower symmetry space group of $P6_1$ and the lattice parameters are listed in Table I. The structure of $Y_{10}[SiO_4]_6N_2$ (N-apatite) is most controversial ever since it was reported.[64,65] Most of the published literature now assumes it has an apatite structure which is a well-known major crystalline phase of oxides. Among the apatite crystals, fluoroapatites $Ca_{10}[PO_4]_6F_2$ and hydroxyapatites $Ca[SiO_4]_6(OH)_2$ are the most well known because of their prominent roles in laser crystal applications[66] and in bioceramics related to the constituents of bones and teeth.[67,68] In the ideal and stoichiometric N-apatite, N occupies the 2*a* site on the *c* axis and is not bonded to any of the Si atoms. However, it has been pointed out that N prefers to be bonded to Si rather than Y.[57] If this is the case then stoichiometric $Y_{10}[SiO_4]_6N_2$ cannot have the exact apatite structure. It will have a structure involving the interchange of N with O ions with a much reduced symmetry.

It is now clear that with the exception of hexagonal $YSiO_2N$, which has some kind of stacking chiral symmetry,[55] the precise atomic positions in the other three quaternary crystals are not available for detailed *ab initio* calculations of electronic structures. It is entirely possible that in these crystals, there are no unique anion positions after all. In order to study the electronic structure and bonding in these crystals, some candidate structures that are close to the real materials must be proposed, and based on these

TABLE II. Candidate models for the exchange of O/N sites from the ideal structure.

	$Y_2Si_3N_4O_3$	$Y_4Si_2O_7N_2$	$Y_{10}[SiO_4]_6N_2$
Wyckoff sites:	N(8*f*),O1(2*c*),O2(4*e*)	See Ref. 12	N(2*a*),O1(6*h*),O2(6*h*),O3(12*i*)
Models			
M1	N1, N2–O1	N1–O1	N1, N2–O1
M2	N1,N2–O2	N1–O2	N1, N2–O2
M3	N1–O1, N2–O2	N2–O1	N1, N2–O3
M4	N3, N4–O1	N2–O2	N1–O1, N2–O2
M5	N3, N4–O2	N1–O1, N2–O2	N1–O2, N2–O3
M6	N3–O1, N4–O2	N1–O2, N2–O1	N1–O3, N2–O1
M7		2 N1–2 O1	
M8		N1–O1, N1–O2	

structures calculations can be carried out. To this end, we have used the density functional theory based Vienna *ab initio* simulation package (VASP)[69,70] to relax several model structures for $Y_2Si_3N_4O_3$, $Y_4Si_2O_7N_2$, and $Y_{10}[SiO_4]_6N_2$. The same approach was used to determine the structure of $YSiO_2N$.[55] In each of the three crystals, six candidate structures were identified which we label as M1, M2, M3, M4, M5, and M6. In $Y_4Si_2O_7N_2$, two additional structures M7 and M8 were later added. The specific sites of O/N exchange in these proposed models are listed in Table II. Although these six or eight models do not exhaust all possible O/N interchanges, we believe they form a reasonable subset for all O/N disordered structures in these crystals.

We next apply the total energy relaxation technique to all models in three crystals with O/N disorder together with the original ideal structure labeled as M0. The relaxation was carried out using the VASP code with local density approximation (LDA) for exchange correlation. We used the ultrasoft Vanderbilt-type pseudopotential[71] as supplied by Kresse and Hafner.[72] For sufficient accuracy, a high-energy cutoff of 600 eV was used. 24, 12, and 24 *k* points in the Monkhorst-Pack scheme were used for Brillouin zone integration, respectively, for the three crystals, which are found to be quite sufficient due to the large unit cells of these crystals. The structures were relaxed via a conjugate-gradient algorithm and analytical expression for Hellmann-Feynman forces to achieve a total energy and force convergence at the level of 0.01 meV and 0.01 eV/Å, respectively. No restrictions were placed on the symmetry of each crystal. For relative comparisons of energies among different candidate models, this level of accuracy is more than sufficient. We have also performed several test calculations using the generalized gradient approximation (GGA) for the structural optimization. The results were quite close to the LDA results except with slightly larger lattice constants. Since the LDA and GGA results differed only slightly and there is no reason to strongly prefer one over the other, at least in the present study for the Y-Si-O-N system, the LDA results were adopted for further analysis.

In $Y_2Si_3N_4O_3$, we find M2, M3, M5, and M6 all have higher energy than M0. M1 and M4 have the same total energy and are lower than M0 by 0.36 eV per cell. M1 is then chosen as the candidate structure for electronic structure calculation. Our most preferred structure is apparently different from the one reported by Fang *et al.*[60] using a similar approach, but with a lower level of accuracy in terms of energy cut off and number of *k* points used. Although the conclusion on the presence of Si-O2N2 and Si-ON3 local bonding units are the same, we do not have the long Y-O bond of 3.1 Å reported in Ref. 60. Our longest Y-O bond in $Y_2Si_3N_2O_3$ is 2.85 Å. This difference could also be partly due to the difference in using either the GGA or LDA potentials.

In $Y_4Si_2O_7N_2$, we find all eight proposed structures have a slightly higher energy than M0. The lowest energy model is M3, which is still higher in energy than M0 by 0.192 eV per cell. So the original structure M0 as reported in Ref. 12 is used for the electronic structure calculation. In the case of $Y_{10}[SiO_4]_6N_2$, we find all six models have substantially lower energy than M0, underscoring the assertion that N prefers to be bonded to Si in N-apatite. Of the six models, M2 has the lowest energy and is lower than M0 by 2.37 eV per cell, or 0.056 eV per atom. The M2 structure is then used for the electronic structure calculation. Because of the interchange of O and N, the symmetry of M1 in $Y_2Si_3N_4O_3$ and M2 in $Y_{10}[SiO_4]_6N_2$ are both reduced to the space group of $P2_1$ (No. 4) and $P2_1/m$ (No. 11), respectively. The lattice parameters and of the relaxed models are listed in Table I. The atomic positions used in the electronic structure calculations for the three crystals are listed in Tables III–V, respectively.

With the atomic positions determined, it is instructive to explore the different local cation-anion bonding configurations occurring in these crystals. Table VI lists all possible cation (Si and Y) and anion (O and N) local nearest neighbor environments. It is quite surprising to see that the common configurations such as the tetrahedral Si-N4, planar N-Si3, and bridging Si-O-Si, which are the backbone structures in binary crystals of α-SiO_2 and β-Si_3N_4, do not occur in these quaternary crystals. Si is always fourfold bonded with all combinations of Si-O_xN_y ($x+y=4$) possible (including Si-N4 in β-Si_3N_4). On the other hand, there are many possible configurations of Y-O_xN_y with coordination numbers ranging from 6 to 9. The maximum number of N nearest neighbors to Y is 5 in $Y_2Si_3N_4O_3$. From the point of view of an anion, O can be either three- or fourfold coordinated. The

TABLE III. Atomic positions of M1 for $Y_2Si_3N_4O_3$: a =7.4238 Å, b=7.6027 Å, c=4.8162 Å, space group: $P2_1$.

Atom	x	y	z
Y1	0.9130	0.8361	0.4985
Y2	0.5983	0.1678	0.5072
Si1	0.2446	0.0023	0.9853
Si2	0.1069	0.6441	0.9367
Si3	0.3915	0.3536	0.9532
O1	0.4082	0.9111	0.1905
O2	0.1145	0.6402	0.2795
O3	0.3951	0.3636	0.2914
N1	0.7436	0.0000	0.1842
N2	0.0913	0.0843	0.2083
N3	0.8299	0.3363	0.2151
N4	0.6507	0.6606	0.1993

most common one is O-SiY3, which occurs in all four quaternary crystals. It is also noted that no coordination of the form O-Si3, O-Si4, O-Si3Y, N-Y3, and N-Si3Y are found in these crystals. These local cation-anion coordination and their implications on the electronic structure and bonding will be further discussed in Sec. III.

III. ELECTRONIC STRUCTURE AND BONDING

The electronic structure and bonding of the quaternary crystals are calculated using the *ab initio* OLCAO method.[62] In principle, the VASP code used for structural determination described in the previous section can also be used to study electronic structure. However, the time-tested OLCAO method in which atomic orbitals are used for basis expansion is a much more versatile and efficient method for analyzing the electronic structure and bonding in complex crystals. This is particularly true for the atom-resolved partial DOS (PDOS), effective charge, and bond order calculations using the Mulliken scheme.[73] In the plane-wave based method, PDOSs are usually obtained by projecting onto some arbitrarily defined atomic basis set or spheres and are somewhat less reliable. The OLCAO method has been successfully applied to the study of $YSiO_2N$,[55] and other crystalline phases in the SiO_2-Y_2O_3-Si_3N_4 phase diagram,[50–56] as well as many other complex ceramic oxides[74–78] and nitrides.[79–85] In the present study, we used a full basis set expansion consisting of atomic orbitals of Y ([Kr] core plus 5*s*, 6*s*, 5*p*, 4*d*, 5*d*), Si ([Ne] core plus 3*s*, 4*s*, 3*p*, 4*p*, 3*d*, 4*d*), and O and N (1*s*, 2*s*, 3*s*, 2*p*, 3*p*). A large number of k points (48, 18, and 48 for $Y_2Si_3N_4O_3$, $Y_4Si_2O_7N_2$, and $Y_{10}[SiO_4]_6N_2$, respectively) in the irreducible portion of the Brillouin zone (BZ) were used for the DOS and optical properties calculations.

TABLE IV. Atomic positions of $Y_4Si_2O_7N_2$ (from Ref. 12): a =7.5601 Å, b=10.4411 Å, c=10.7623 Å; space group: $P2_1/c$.

Atom	x	y	z
Y1	0.8328	0.1214	0.4290
Y2	0.3358	0.1227	0.4173
Y3	0.5281	0.4139	0.3107
Y4	0.0232	0.4024	0.2885
Si1	0.7352	0.1882	0.1321
Si2	0.1552	0.1851	0.1161
N1	0.9394	0.2402	0.1092
N2	0.7175	0.0354	0.1703
O1	0.2105	0.0314	0.1683
O2	0.7154	0.2753	0.2513
O3	0.2824	0.2653	0.2442
O4	0.5774	0.2333	−0.0132
O5	0.1644	0.2203	−0.0262
O6	0.4318	0.4943	0.1074
O7	0.9185	0.5192	0.0973

TABLE V. Atomic positions of M2 of $Y_{10}[SiO_4]_6N_2$: a =9.1246 Å, b=9.0413 Å, c=6.7302 Å, space group: $P2_1/m$.

Atom	x	y	z
Y1	0.3271	0.5032	0.6629
Y2	0.7605	0.7500	0.9918
Y3	0.2319	0.7500	0.2459
Y4	0.0103	0.7500	0.7634
Si1	0.9731	0.7500	0.3728
Si2	0.4017	0.7500	0.0347
Si3	0.6319	0.7500	0.6042
O1	0.0031	0.7500	0.0011
O2	0.3185	0.7500	0.8342
O3	0.5181	0.7500	0.6933
O4	0.8632	0.7500	0.4721
O5	0.6030	0.7500	0.1287
O6	0.5266	0.7500	0.4000
O7	0.8939	0.5575	0.2449
O8	0.3456	0.5574	0.1005
O9	0.7548	0.5616	0.6612
N	0.1747	0.7500	0.4870

A. Density of states and partial density of states

The calculated total DOS of $Y_2Si_3N_4O_3$, $Y_4Si_2O_7N_2$, and $Y_{10}[SiO_4]_6N_2$ are shown in Fig. 3. All three crystals are insulators with band gaps of 3.40, 3.19, and 3.70 eV, respectively. These band gaps are considered to be lower limits since it is well known that LDA calculations generally underestimate the band gap of insulators. The states near the top of the valence band (VB) come mostly from the nonbonding orbitals of N and show some very distinctive features. The widths of the upper VB for the three crystals are 9.2, 8.1, and 7.4 eV, respectively. The atom-resolved PDOS of these three crystals are shown in Figs. 4–6, respectively. These spectra are very rich in structure and can be best explained by the local bonding environments of each type of atoms elaborated in the previous section. For example, if a

TABLE VI. Possible cation to anion bonding coordination in the four quaternary crystals.

Si bonding	Crystals	O bonding	Crystals
Si-O4	$Y_{10}[SiO_4]_6N_2$	O-Si2 (bridging)	None (only in SiO_2 and Si_2N_2O)
Si-O3N	$Y_4Si_2O_7N_2$, $Y_{10}[SiO_4]_6N_2$	O-SiY2	$Y_4Si_2O_7N_2$
Si-O2N2	$Y_2Si_3N_4O_3$, $Y_4Si_2O_7N_2$, $YSiO_2N$	O-SiY3	$Y_2Si_3N_4O_3$ $Y_4Si_2O_7N_2$ $YSiO_2N$, $Y_{10}[SiO_4]_6N_2$
Si-ON3	$Y_2Si_3N_4O_3$	O-Si2Y2	$Y_2Si_3N_4O_3$
Si-N4	None (only in Si_3N_4)	O-Y3	$Y_{10}[SiO_4]_6N_2$
		O-Y4	$Y_4Si_2O_7N_2$
Y bonding	Crystals	N bonding	Crystals
Y-O6	$Y_{10}[SiO_4]_6N_2$	N-Si3	None (only in Si_3N_4 and Si_2N_2O)
Y-O7	$Y_4Si_2O_7N_2$	N-Si2Y2	$Y_2Si_3N_4O_3$, $Y_4Si_2O_7N_2$, $YSiO_2N$,
Y-O3N5	$Y_2Si_3N_4O_3$	N-SiY3	$Y_4Si_2O_7N_2$, $Y_{10}[SiO_4]_6N_2$.
Y-O5N	$Y_4Si_2O_7N_2$		
Y-O5N2	$Y_4Si_2O_7N_2$		
Y-O5N3	$Y_2Si_3N_4O_3$		
Y-O6N2	$YSiO_2N$		
Y-O6-N	$Y_{10}[SiO_4]_6N_2$		
Y-O8N	$Y_{10}[SiO_4]_6N_2$		

strong peak occurs at the same energy in the PDOS of a particular Si atom and a particular O atom, it implies that these two atoms are strongly bonded. In the DOS and PDOS plots of the Y-Si-O-N crystals, we observe several general features that are shared by all three crystals. In the VB region, the lowest peak centered around −21 eV is from the semicore Y-4*p* levels. The structures in the energy range of −17.5 to −20 eV come from the O-2*s* levels and their interacting counterparts. Similarly, the structures within the range from −13 to −16 eV come from the N-2*s* levels and their interacting counterparts. Above the −10 eV, the states comprise of a mixture of the O and N bonding and nonbonding orbitals involving hybridized sp^3 orbitals. The bonding states are predominately from the Si-O and Si-N pairs with some minor participation from Y-5*s* and Y-5*p* orbitals. The O bonding states are on the lower edge of the upper VB while the N nonbonding states are usually at the top of the VB. In the conduction band (CB) region, the states are much more delocalized and consist of the antibonding states of the corresponding bonding states in the VB. They are mostly from cations with Y-4*d* states dominating near the bottom of the CB. The Si antibonding states are generally at a higher energy level around 10 eV. The structures in the CB PDOS are more sensitive to the local environment of a particular atom than the VB PDOS.

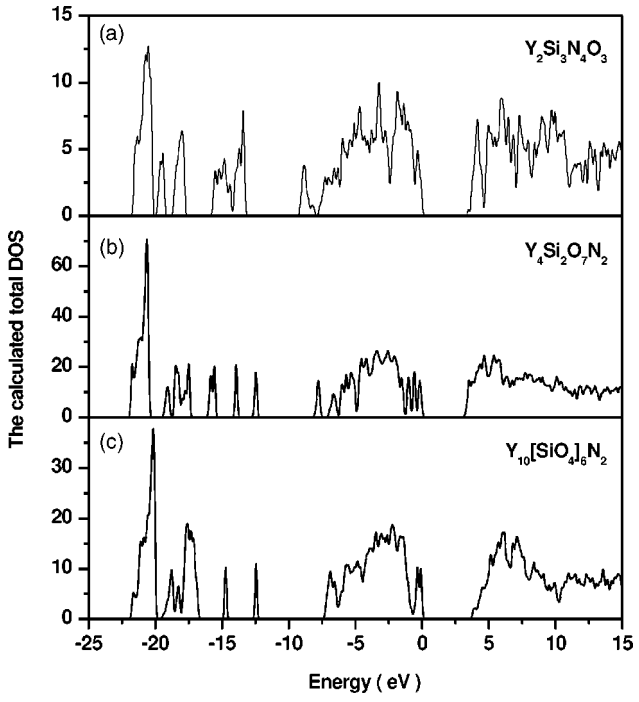

FIG. 3. The calculated total DOS of (a) $Y_2Si_3N_4O_3$, (b) $Y_4Si_2O_7N_2$, and (c) $Y_{10}[SiO_4]_6N_2$.

With the general features of Fig. 3 summarized above, we can now discuss specific features in each crystal that are finger prints of their local coordination. Figure 4 shows the PDOS of $Y_2Si_3N_4O_3$ for all crystallographically nonequivalent sites of model M1. The difference in the PDOS of Y1 and Y2 is due to the fact that Y1 bonds to 3 O and 5 N while Y2 bonds to 5 O and 3 N. Nevertheless, their differences are small. Si1 and Si2 both bond to 1 O and 3 N and their PDOS are similar, but are slightly different from that of Si3, which bonds to 2 O and 2 N. The PDOS for O1 is significantly different from that of O2 and O3 especially in the O-2*s* peak position and in the lower VB region. This is because O1 bonds to 2 Y and 2 Si while O2 and O3 bond to 3Y and one Si. Since Si-O is a stronger bond than the Y-O bond, the

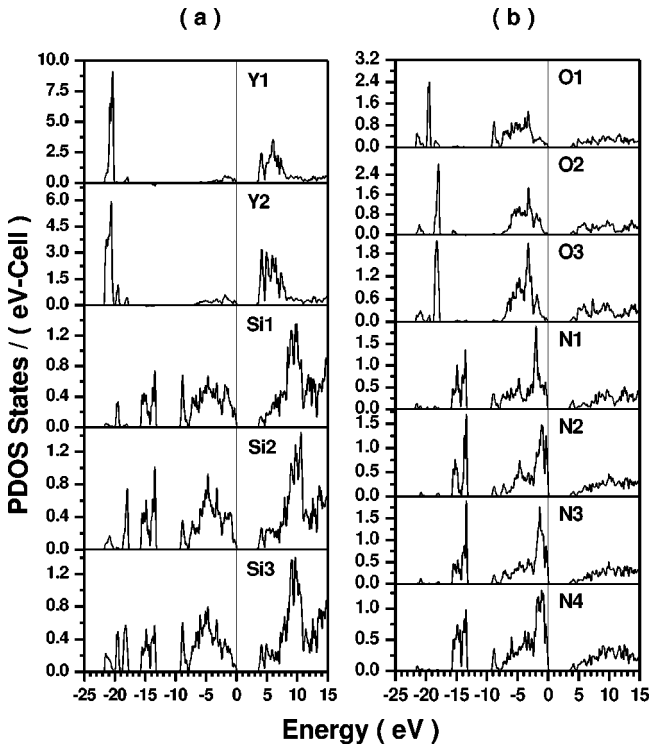

FIG. 4. The calculated PDOS of $Y_2Si_3N_4O_3$: (a) cations and (b) anions.

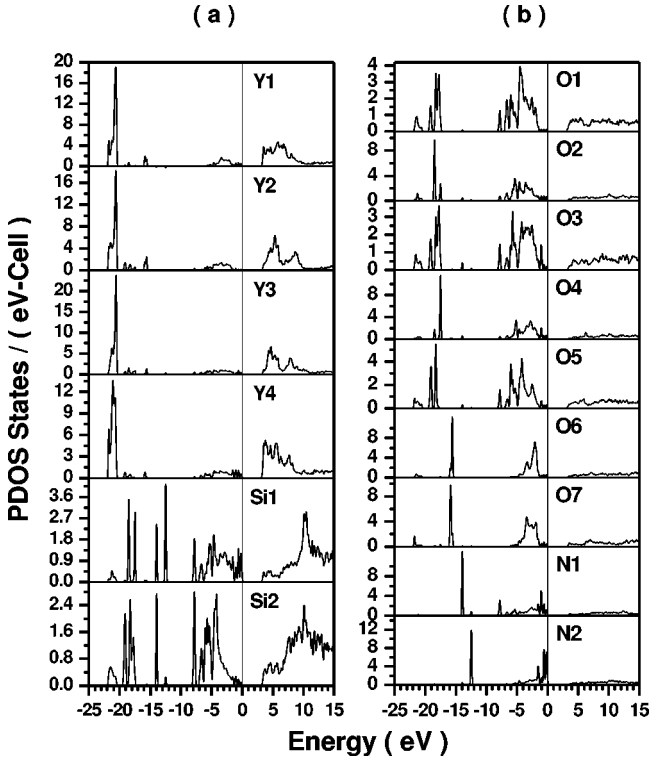

FIG. 5. The calculated PDOS of $Y_4Si_2O_7N_2$: (a) cations and (b) anions.

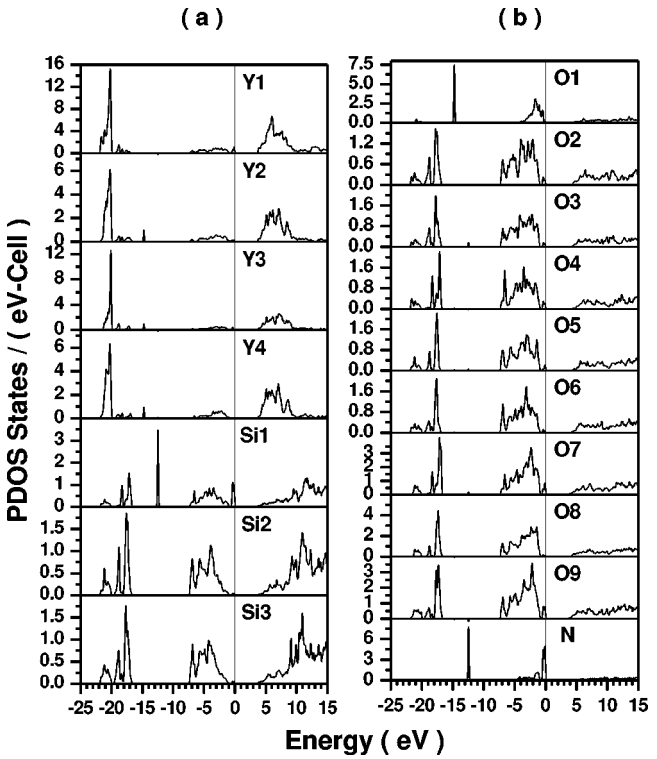

FIG. 6. The calculated PDOS of $Y_{10}[SiO_4]_6N_2$: (a) cations and (b) anions.

spectral weight of PDOS in O1 shifts to the lower binding energy than those of O2 and O3. The PDOS of the four N atoms show no large variations since they all bond to 2 Y and 2 Si. Minor differences in their PDOS can be traced to the slight differences in the interatomic bond lengths and the second nearest neighbor (SNN) effects.

The PDOS for $Y_4Si_2O_7N_2$ are shown in Fig. 5. They are very rich in structure and the main features can be summarized as follows: (1) as can be seen from Table IV, there are four different Y ions with specific bonding of Y1-N2O6, Y2-O7, Y3-NO5, and Y4-N2O5. Their PDOS differ mostly in the CB region. This illustrates the sensitivity of the CB PDOS spectra to the local bonding configurations. (2) There are two independent Si and N sites, Si1 bonds to two N (N1 and N2) and 2 O, while Si2 bonds to 1 N (N1) and 3 O. This feature is clearly delineated by the two sharp peaks at −14 and −12.5 eV, respectively, in both PDOS of Si1 and Si2, as well as the different positions of N-2*s* peak in the PDOS of N1 and N2. These differences in the local bonding configurations also resulted in significant different features at the top of the VB of Si1 and Si2. (3) There are seven crystallographically nonequivalent O ions that can be classified into two groups. The Os in the first group (O1, O2, O3, O4, O5) bond to 1 Si and 3 Y. Their PDOS are very similar. Still, slight differences in the O-2s peak position and some additional features near the top of the VB can be found and can be attributed to the SNN effect. The O atoms in the second group (O6 and O7) all bond to 4 Y and their PDOS are very different from that of the first group. The O-2*s* peak in the second group is at a higher binding energy of −15.7 eV and the PDOS in the upper VB are sharper and cover a shorter range of only about 5 eV. These features reflect the relatively

TABLE VII. Summary of calculated Mulliken effective charges Q^* (total number of valence electrons).

Crystals	$Y_2Si_3N_4O_3$	$Y_4Si_2O_7N_2$	$YSiO_2N$	$Y_{10}[SiO_4]_6N_2$
Y	1.629, 1.939	1.996, 2.002	1.881, 1.890	2.009, 1.962
		1.980, 2.019	⋯	1.968, 1.931
Si	2.807, 2.912, 2.826	2.866, 2.742	2.795, 2.792	2.850, 2.696, 2.709
O	6.691, 6.661, 6.672	6.685, 6.696	6.703, 6.691	6.600, 6.679, 6.676
	⋯	6.690, 6.678	6.699	6.664, 6.685, 6.684
	⋯	6.708, 6.605, 6.595	⋯	6.665, 6.686, 6.681
N	5.910, 5.883, 5.882	5.904, 5.835	5.931, 5.936	5.655

weak Si-O bonds. (4) The PDOS of N1 and N2 are also quite different. The N-2*s* peaks are at −14 and −12.5 eV, respectively, collaborating with the peaks in the PDOS of Si1 at the same locations. Their PDOS in the VB region are also very different. N1 has its spectral weight at a lower binding energy than N2.

The electronic structure of $Y_{10}[SiO_4]_6N_2$ deserves particular attention. As mentioned in Sec. I, a preliminary calculation on the idealized N-apatite structure has been reported.[56] It shows two different Y sites, one Si site and three different O sites (O1, O2, O3) with O3 somewhat different from O1 and O2. The N is at the 2*a* site, and bonds only to three Y ions, resulting in a strong N-2*s* peak at −11.5 eV and a set of N-2*p* bands residing in what supposed to be the wide band gap of the SiO_2 backbone.[56] Figure 6 shows the PDOS of the newly relaxed structure (M2), which has a lower energy and with N bonds to Si. The PDOS of all the crystallographically nonequivalent sites are shown in Fig. 6 even though many of them have almost identical local bonding structure as a result of the reduction in crystal symmetry from the ideal apatite structure. As can be seen, the PDOS of 4 Y ions are not very different. Only Y1 (bonded to 8 O and 1 N) is slightly different from other three (bonded either to 7 O or 6 O and 1 N). The same can be said to the PDOS of O. With the exception of O1, which now occupies the 2*a* site along the *c* axis after interchanging with N and bonds to 3 Y ions, all other Os bond to 1 Si and 3 Y and have very similar PDOS. The weakly bonded O1 has its PDOS totally different from other eight Os and this is manifested in the strongly localized O-2*s* peak at −14.8 eV as well as a much reduced width of the upper VB. It should also be pointed out that the PDOS of O1 is very similar to the PDOS of O6 and O7 of $Y_2Si_3N_4O_3$ in Fig. 4 with similar local coordination. There are again three types of Si (Si1, Si2, and Si3). Si1 bonds to 1 N and 3 O and is characterized by a sharp Si-N-2*s* bonding peak at −12.5 eV. Si2 and Si3 both bond to 4 O and have almost identical PDOS. For the N atom that now bonds to 1 Si and 3 Y instead of 3 Y in the ideal apatite structure, there is a sharp N-2*p* nonbonding peak at the top of the VB in addition to the N-2*s* bonding peak at −12.5 eV. As a result, the band gap in the present case is greatly enlarged from 1.3 eV in the previous calculation[56] to the present value of 3.70 eV.

B. Effective charges and bond order

One of the most useful features of the OLCAO method is the provision of quantitative information on the effective charges Q^*_α on each atom and the strength of the bond between any pair of atoms in the form of bond order (BO) values $\rho_{\alpha,\beta}$. Here, the effective charges Q^*_α is the total number of calculated valence electrons on each atom and is always a positive number. Q^*_α and $\rho_{\alpha,\beta}$ provide information on charge transfer and the relative strengths of various interatomic bonds within a crystal. Q^*_α and $\rho_{\alpha,\beta}$ are calculated from the *ab initio* eigenvector coefficients $C^n_{i\alpha}$ and overlap integrals $S_{i\alpha,j\beta}$ in accordance with the Mulliken scheme[73]

$$Q^*_\alpha = \sum_i \sum_{n,occ} \sum_{j,\beta} C^{*n}_{i\alpha} C^n_{j\beta} S_{i\alpha,j\beta}, \tag{1}$$

$$\rho_{\alpha\beta} = \sum_{n,occ} \sum_{i,j} C^{*n}_{i\alpha} C^n_{j\beta} S_{i\alpha,j\beta}. \tag{2}$$

For effective charge and BO calculations, a minimal basis set is generally used since the Mulliken scheme works best with a more localized basis set. The calculated results for Q^*_α and $\rho_{\alpha,\beta}$ for the four quaternary crystals including those of $YSiO_2N$ (Ref. 55) are listed in Tables VII and VIII, respectively. Also listed are the corresponding bond lengths (BLs). In general, the BO values scale with BL but not always since the calculation based on Eqs. (1) and (2) is a quantum mechanical one in which the wave functions extend over all atoms in the crystal.

From Table VII for the calculated effective charges, it can be seen that: (1) the charge transfer from Y to O and N is about one electron except in the case of Y1 in $Y_2Si_3N_4O_3$ where Q^* for Y1 is 1.63. This difference can actually be seen from the PDOS of Fig. 4 where the Y-4*p* peak is at a higher energy than those of other Y ions in the four crystals indicating a more positive Y ion. (2) The effective charge of the Si atom ranges from 2.70 in Si2 of $Y_{10}[SiO_4]_6N_2$ to 2.89 of Si1 in $Y_2Si_3N_4O_3$. These differences reflect the different types of local Si-O_xN_y bonding discussed earlier. For example, the Si2 in $Y_{10}[SiO_4]_6N_2$ is bonded to four O and Si1 in $Y_4Si_2O_7N_2$ is bonded to 1 N and 3 O. Likewise, Si1 in $Y_4Si_2O_7N_2$ is the Si ion which bonds to 2 N and 2 O. Since N is less electronegative than O, there is less charge transfer from Si if it bonds to more N atoms and will have a higher covalency. (3) The deviations of Q^* of anions are somewhat less prominent. Q^* for O ranges from 6.60 to 6.70 in $Y_4Si_2O_7N_2$. Q^* for N ranges from 5.91 in $Y_2Si_3N_4O_3$ to 5.94 in $YSiO_2N$. Thus the charge transfers in quaternary Y-Si-ON crystals cover a relatively narrow range depending on actual

TABLE VIII. Summary of calculated bond order values in four quaternary crystals. The numbers in parentheses are the bond lengths in Å. For $Y_4Si_2O_7N_2$ and $Y_{10}[SiO_4]_6N_2$, the BO for Y-O BO are the averaged values over the five groups as explained in the text. The integer number in the square bracket is the number of bonds in that group.

Crystals	$Y_2Si_3N_4O_3$	$Y_4Si_2O_7N_2$	$YSiO_2N$	$Y_{10}[SiO_4]_6N_2$
Y-O	0.132 (2.359)	Averaged:	0.095 (2.593)	Averaged:
	0.095 (2.555)	0.172 (2.211)[3]	0.088 (2.595)	0.203 (2.204)[5]
	0.094 (2.509)	0.159 (2.280)[8]	0.175 (2.257)	0.172 (2.271)[5]
	0.042 (2.852)	0.150 (2.317)[4]	0.087 (2.637)	0.136 (2.313)[4]
	0.131 (2.355)	0.139 (2.394)[3]	0.176 (2.257)	0.119 (2.394)[9]
	0.134 (2.377)	0.066 (2.694)[5]	0.088 (2.582)	0.079 (2.614)[5]
	0.136 (2.361)	…	0.179 (2.292)	…
	0.105 (2.509)	…	0.093 (2.568)	…
	…	…	0.088 (2.582)	…
Y-N	0.139 (2.331)	0.161(2.330)	0.142 (2.404)	0.211 (2.253)
	0.086 (2.695)	0.070(2.767)	0.145 (2.380)	0.130 (2.476)
	0.180 (2.379)	0.240 (2.315)	0.133 (2.420)	…
	0.169 (2.356)	0.135 (2.481)	…	…
	0.062 (2.768)	0.250 (2.318)	…	…
	0.162 (2.282)	…	…	…
	0.111 (2.563)	…	…	…
	0.184 (2.327)	…	…	…
Si-O	0.223 (1.713)	0.270 (1.621)	0.301 (1.655)	0.271 (1.639)
	0.355 (1.653)	0.266 (1.677)	0.303 (1.644)	0.280 (1.651)[2]
	0.239 (1.697)	0.261 (1.704)	0.305 (1.639)	0.314 (1.590)
	0.372 (1.630)	0.294 (1.618)	0.305 (1.639)	0.302 (1.607)
	…	0.313 (1.600)	…	0.316 (1.610)[2]
	…	…	…	0.317 (1.593)
	…	…	…	0.298 (1.616)
	…	…	…	0.318 (1.603)[2]
Si-N	0.389 (1.684)	0.343 (1.732)	0.367 (1.693)	0.474 (1.615)
	0.393 (1.682)	0.427 (1.664)	0.364 (1.698)	…
	0.388 (1.686)	0.378 (1.707)	0.365 (1.698)	…
	0.332 (1.664)	…	0.365 (1.698)	…
	0.374 (1.692)	…	…	…
	0.363 (1.700)	…	…	…
Cell bond order:	12.304	26.203	14.088	18.185

local configurations, and are consistent with the PDOS diagrams shown in Figs. 4–6.

Table VIII lists the calculated BO values for Y-O, Y-N, Si-O, and Si-N bonds in the four crystals. The values for Y-O in $Y_4Si_2O_7N_2$ and $Y_{10}[SiO_4]_6N_2$ are grouped because too many different bonds occur (23 and 28 Y-O bonds, respectively). It is not practical to list all of them individually. Accordingly, the BO and BL values in $Y_4Si_2O_7N_2$ and $Y_{10}[SiO_4]_6N_2$ are averaged over five groups according to their BLs: (1) less than 2.25 Å, (2) between 2.25 and 2.30 Å, (3) between 2.30 and 2.35 Å, (4) between 2.35 and 2.45 Å, and (5) greater than 2.45 Å. All other Y-O bonds are listed individually. Generally speaking, the BO values scale with BL, which is the basis of less rigorous estimations such as in the bond valence sum model.[86] The present calculation of BO is entirely quantum mechanical using *ab initio* wave functions. The BO values are affected by the presence of other nearby atoms or bond angles, not just the two atoms that form a bond. It is obvious that Si-N is the strongest bond in the Y-Si-O-N system. The large BO value of 0.47 for Si-N is in $Y_{10}[SiO_4]_6N_2$. This is the main reason for the ideal apatite structure to be invalid in this crystal. Largest BO of 0.43 for Si-N also occurs in $Y_4Si_2O_7N_2$. All other Si-N BO values are greater than 0.33. The Si-O bonds are only slightly weaker than the Si-N bonds. Their BO values range from 0.22 to 0.37. Both the upper and the lower limits occur in $Y_2Si_3N_4O_3$, where each Si atom has two stronger Si-O bonds and two weaker Si-O bonds. The Y-N bonds also have considerable BO values of up to 0.24, and 0.25 (in $Y_4Si_2O_7N_2$) and 0.21 (in $Y_{10}[SiO_4]_6N_2$). It is worth noting that the BL of

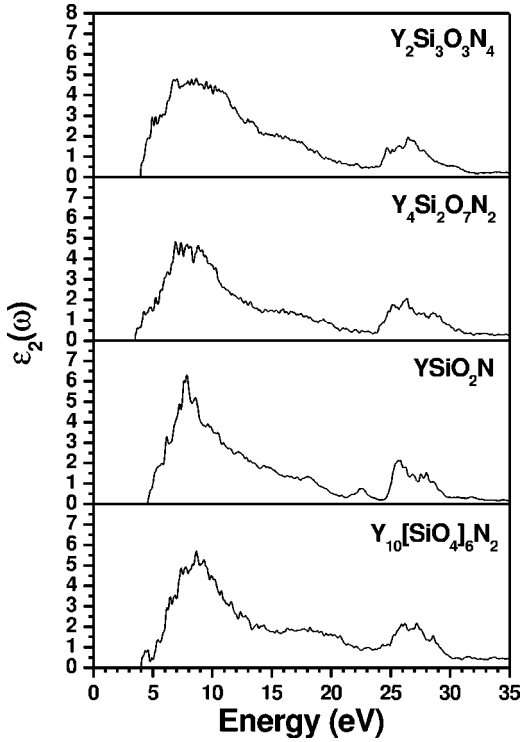

FIG. 7. Comparison of the calculated imaginary parts of the dielectric functions for the four quaternary crystals.

Y-N (2.253 Å) in $Y_{10}[SiO_4]_6N_2$ is actually shorter than those in $Y_4Si_2O_7N_2$ (2.315 and 2.318 Å), yet the former has a smaller BO value. The Y-O bonds are the weakest of all cation-anion bonds in the Y-Si-O-N system mainly because of the larger Y-O BLs. Their range from a low value of 0.042 in $Y_2Si_3N_4O_3$ to a respectable value of 0.203 in $Y_{10}[SiO_4]_6N_2$, which is actually larger than the BO for the Al-O bonds in the Y-Al-O system.[74,75] As pointed out earlier, there are many more Y-O bonds than other cation-anion bonds. Hence, the overall contribution of Y-O bonding to crystalline cohesion should not be overlooked. This has not been the case in much of the published literature, which usually assumes the Y-O bonding to be too weak to be of any consequence.

For the crystal as a whole, a more meaningful quantity is the total cell bond order which is the sum of all bond order values in the crystal. Since the four quaternary crystals contain different number of atoms and bonds, a much more useful concept is the average cell bond order per unit volume. These numbers are also listed in Table VIII. It turns out that $Y_2Si_3N_4O_3$ has the highest value of 0.045 electron/(Å)^3 for the cell BO per unit volume. The other three crystals have the values of 0.032, 0.036, and 0.037 electron/(Å)^3. So we may conclude that $Y_2Si_3N_4O_3$ crystal has the strongest crystal bonding among the four crystals. This is most likely due to its higher N content.

IV. OPTICAL PROPERTIES

The optical properties of the four Y-Si-O-N quaternary crystals are also calculated based on the modeled structures. We used the so-called extended basis set within the OLCAO method by supplementing additional atomic orbitals to the full basis set used in the electronic structure calculation. This provides more accurate Bloch functions for states in the upper part of the CB. The optical properties can be best represented by the frequency-dependent complex dielectric functions. In our approach, the imaginary part of the dielectric function $\varepsilon_2(\omega)$ is calculated first according to

$$\varepsilon_2(\hbar\omega) = \frac{e^2}{\pi m\omega^2}\int_{BZ} dk^3 \sum_{n,l} |\langle\psi_n(\mathbf{k},\mathbf{r}^{\sim})| - i\hbar\,\nabla\,|\psi_l(\mathbf{k},\mathbf{r}^{\sim})\rangle|^2 f_l(\mathbf{k})[1-f_n(\mathbf{k})] \times \delta(E_n(\mathbf{k}) - E_l(\mathbf{k}) - \hbar\omega), \quad (3)$$

where $f_1(\mathbf{k})$ is the Fermi distribution function and $\hbar\omega$ is the frequency of transition. The real part, $\varepsilon_1(\omega)$, is obtained from the imaginary part by Kramers-Kronig conversion. The transition frequency is limited to about 35 eV, since above that energy, the accuracy of the wave functions can no longer be guaranteed even with an extended basis set. The energy loss function (ELF) was obtained from the imaginary part of the inverse of the complex dielectric function, or ELF $=\mathrm{Im}[(\varepsilon_1(\omega)+i\varepsilon_2(\omega))^{-1}]$. The peaks in ELF are identified as plasmon frequencies ω_p for collective excitations of the electrons in the solid.

The calculated complex dielectric functions and the electron ELF of the four quaternary crystals are shown in Figs. 7–9, respectively. As can be seen, $\varepsilon_2(\omega)$ curves have thresholds of transition close to the band gap values of the respective crystals. They rise swiftly and peak around 8–9 eV. The peak is quite broad in $Y_2Si_3N_4O_3$ but is fairly sharp in $YSiO_2N$ (at 7.9 eV), a fact that could be related to the absence of O/N disorder in the later crystal. Beyond 10 eV, the $\varepsilon_2(\omega)$ spectra gradually decrease until at about 24–25 eV, they start to rise again with another broad peak between 25 and 29 eV. These peaks originate from transitions from the semicore Y-4*p* bands at −21 eV to the empty CB states.

The real parts of the dielectric functions $\varepsilon_1(\omega)$ of the four crystals are shown in Fig. 8. Their general shapes are very similar since the $\varepsilon_2(\omega)$ spectra are quite similar. The refractive index of an insulating crystal can be related to the square root of the electronic part of the dielectric constant at zero frequency, or $\varepsilon_0=\varepsilon_1(\hbar\omega=0)$. From Fig. 8, we can estimate the refractive indices of the four crystals to be 2.09, 1.98, 1.94, and 2.02, respectively. Figure 9 shows the electron energy loss functions of the four crystals. In general, they are two plasmon frequencies within the 0–35 eV region. These plasmon peak values are listed in Table IX. Also listed in Table IX are other parameters relevant to optical properties of the four Si-Yi-O-N quaternary crystals.

There are two primary reasons for the calculation of optical properties of these quaternary crystals. First, it has been pointed out in Sec. I that Si_3N_4 ceramic has applications in microelectronics. The main goal is to develop materials with high dielectric constant since the current technology based on the use of SiO_2 will soon reach its theoretical limit, unless other compatible materials with higher dielectric constants can be found.[87] SiO_xN_y with appropriate composition modi-

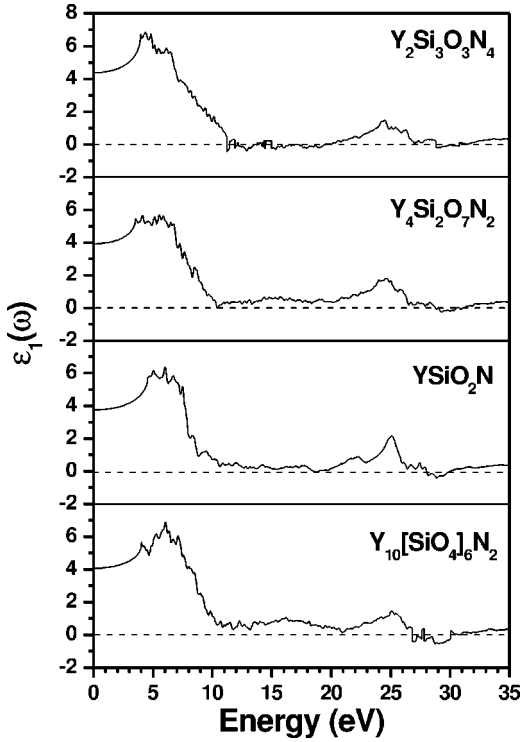

FIG. 8. Comparison of the calculated real parts of the dielectric functions for the four quaternary crystals.

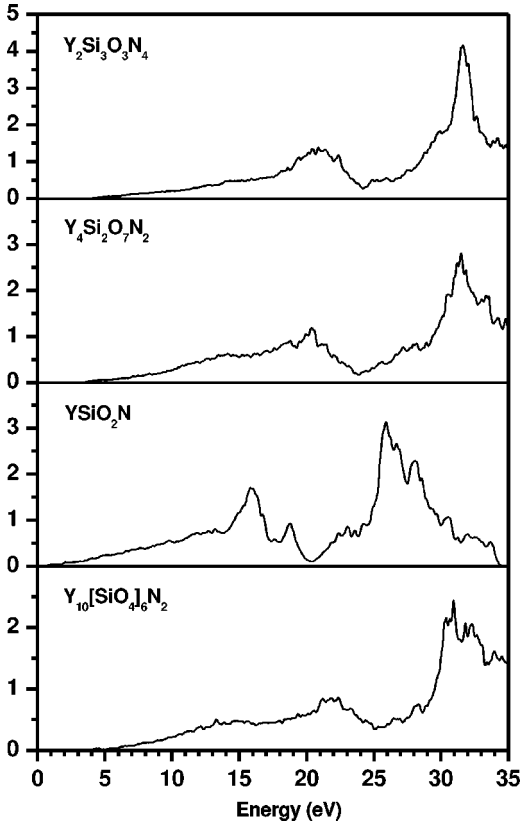

FIG. 9. Comparison of the calculated electron-energy-loss functions for the four quaternary crystals.

fications by adding other elements is one of the viable candidates.[88] The other material being considered is Zr-silicates.[89,90] The present calculation of ε_0 for the four quaternary crystals gives some useful estimation on the range of the possible dielectric constants (electronic contributions) that can be obtained from these materials in relation to different O/N ratios. The specific bonding considerations discussed in Sec. III can also provide some insight into the ionic contribution to the dielectric constants.

The second important aspect of the optical properties is that it can be used as the starting point to estimate the London dispersion force between ceramic grains which has its origin in the electrodynamics of induced dipoles. This is the most important part of the van der Waals (vdW) attractive force, the balancing with other forces for the formation of IGF discussed in Sec. I. The Haymaker constant, which scales with the vdW force, can be calculated using the continuum theory of Dzayloshinski *et al.*[91–93] The basic quantity required is the London dispersion transformation of the frequency-dependent dielectric function.[93] In the simplest approach, the refractive index of materials can be used for such estimations.[94] French[95,96] has used the experimentally determined optical spectra from vacuum ultraviolet spectroscopy to obtain the Haymaker constants of many different combinations of ceramic crystals with different intervening media using the Lifshitz theory. Since no experimental optical spectra for the Y-Si-O-N quaternary crystals are available, at least at the present time, the theoretically derived frequency-dependent dielectric functions can be used as a substitute for such calculations.

V. DISCUSSION AND CONCLUSIONS

We have completed a comprehensive study of the electronic structure and bonding of the four known quaternary crystals in the Y-Si-O-N system. This is a major step in the fundamental understanding of this class of complex ceramics beyond the past work, the field of which tends to concentrate on the processing and characterization of microstructures in these materials. They are all insulators with fairly large band gaps. In the cases where O/N disorder exists, the atomic positions used in the calculation were determined by *ab initio* modeling. It is shown that the nominal crystal structures of $Y_4Si_2O_7N_2$ and $Y_{10}[SiO_4]_6N_2$ no longer hold true. The real structures would have a lower symmetry and may even be amorphous in nature or contain defects. Indeed, it has been suggested in the past that N-apatite could actually be $Y_{10}[SiO_3N]_6\square_2$ in which the 2*a* site is empty and all N atoms are bonded to Si or other combinations.[10] Such defective structures can also be studied by the *ab initio* modeling technique used here. However, the N/O ration in $Y_{10}[SiO_3N]_6\square_2$ is no longer the same as in $Y_{10}[SiO_4]_6N_2$, and it requires other experimental probes to pin down the most probable structure. In addition to the modeling of impurity and defect structures in the Y-Si-O-N system, it is also desirable to extend the current study to other quaternary systems in the phase diagrams of say, SiO_2-Si_3N_4-MgO, SiO_2-Si_3N_4-CaO, or Y containing Si-Al-O-N systems (Y-Si-Al-O-N) to have an even broader picture of the structural ceramics.

TABLE IX. Summary of calculated optical properties of quaternary crystals.

Crystals	$Y_2Si_3N_4O_3$	$Y_4Si_2O_7N_2$	$YSiO_2N$	$Y_{10}[SiO_4]_6N_2$
E_g (eV)	3.40	3.19	4.40	3.70
$\varepsilon_1(0)$	4.38	3.91	3.75	4.07
Refractive index n	2.09	1.98	1.94	2.02
Main peak in $\varepsilon_2(\omega)$ (eV)	8.37	7,81	7.80	8.51
ω_p (eV)	21.0, 31.6	20.3, 31.2	20.0, 22.8, 30.0	22.0, 30.9
VB width (eV)	9.2	8.1	8.9	7.4

In this study, a variety of local cation/anion bonding configurations are identified in the Y-Si-O-N system and discussed in the context of calculated PDOS, the charge transfer inferred from effective Mulliken charges, and bond order values. These local bonding structures are very likely to exist in the interior or at the boundary of the metal-doped IGF in polycrystalline Si_3N_4. So the information we obtained could be used as a useful reference in the construction of realistic structural models for IGF. It is shown that the Si-N bond has the strongest bond strength, followed by the Si-O. However, the bonding of the Y-O and Y-N pairs should not be ignored in the analysis. Y-N and Y-O bonds have considerable strength in spite of relatively large bond distances. Furthermore, Y has a higher coordination number and there are many more Y-O and Y-N bonds that can contribute to the overall crystal cohesion. The optical property calculation shows that these crystals all have very similar optical spectra. A slight variation can result in small difference in their refractive indices. Such a difference is most likely related to the different concentration ratios of cation/anion or O/N, and not so much to the actual crystal structures.

A promising area for further study of the Y-Si-O-N system is the characterization of these materials by means of x-ray absorption near edges spectroscopy (XANES) or the energy loss near edge spectroscopy (ELNES). The XANES/ELNES spectra of the Si-*K*, Si-$L_{2,3}$, Y-*K*, Y-$M_{3,4}$, O-*K*, and N-*K* edges in these materials are very sensitive to the rich local environment of the cations and anions described in this paper, and could be a better alternative to the NMR techniques used so far in determining the local structures.[21–25] The extensive overlap of the chemical shifts in the magic-angle spinning NMR spectra makes unambiguous assignment of local structural unit a rather difficult task.[22] Using the supercell method,[97] which accounts for the presence of the core-hole, accurate XANES/ELNES spectra can be obtained and compared. In conjunction with the experimentally measured spectra on these systems, a much deeper understanding on the local bonding structure in these crystals is expected. So far, such calculations have only been applied to the binary crystals[98–101] of the phase diagrams of Fig. 1 and to Si_2N_2O.[101] Similar calculations on the ternary and quaternary crystals are being contemplated as soon as the required computational resources become available. Experimental ELNES measurements on polycrystals containing IGF have been attempted.[35] However, the low-energy resolution of the spectra and the lack of any structural information about IGF preclude any definitive conclusions.

The current results provide a more complete set of quantitative data for realistic statistical analysis of the structure-properties relationship in the Y-Si-O-N system. Hopefully, this will shed some light on the nature of IGFs and other microstructures in polycrystalline nitrogen ceramics that will eventually lead to their wider applications in modern technology. We intend to use the present results to do more realistic modeling of IGF structures in polycrystalline Si_3N_4, or at a larger scale, the joining of polycrystalline Si_3N_4 using refractory oxynitrides.[102] The understanding of the nanoscale microstructural characteristics associated with IGF and the precise mechanism that controls the mechanical properties of sintered bulk ceramics is one of the most outstanding problems in ceramic science. A computational approach to this complex problem is only at the beginning. Finally, in this paper, we have demonstrated the effectiveness of combining two different *ab initio* methods, thereby overcoming the limitations of each individual method in attacking problems of great complexity.

ACKNOWLEDGMENTS

Work is supported by NSF Grant No. DMR-0016 in collaboration with NANOAM Project of EU-CODIS (Grant No. G5RD-CT-2001-00586). It is also partially supported by the U.S. Department of Energy under Grant No. DE-FG02-84DR45170. This research used the resources of NERSC supported by Office of Science of DOE under Contract No. DE-AC03-76SF00098.

*Corresponding author. Email address: chingw@umkc.edu

[1] F. L. Riley, J. Am. Ceram. Soc. **83**, 245 (2000).

[2] L. J. Gauckler, S. Prietzel, G. Bodemer, and G. Petzow, in *Nitrogen Ceramics*, edited by F. L. Riley (Noordhoff, Leyden, The Netherlands, 1977), pp. 529–537.

[3] I. MacLaren, L. K. L. Falk, A. Diaz, and S. Hampshire, J. Am. Ceram. Soc. **84**, 1601 (2001).

[4] T. Ekstrøm and M. Nygren, J. Am. Ceram. Soc. **75**, 259 (1992).

[5] K. H. Jack and W. I. Wilson, Nature (London), Phys. Sci. **238**, 28 (1972).
[6] Y. Oyama, Jpn. J. Appl. Phys. **10**, 1637 (1971).
[7] W. Y. Ching, M-.Z. Huang, and S. D. Mo, J. Am. Ceram. Soc. **83**, 780 (2000).
[8] R. R. Wills, S. Holmquist, J. M. Wimmer, and J. A. Cunningham, J. Mater. Res. **11**, 1305 (1976).
[9] F. F. Lange, S. C. Singhal, and R. C. Kuznicki, J. Am. Ceram. Soc. **60**, 249 (1977).
[10] L. J. Gauckler, H. Hohnke, and T. Y. Tien, J. Am. Ceram. Soc. **63**, 35 (1980).
[11] P. E. D. Morgan, P. J. Carroll, and F. F. Lange, Mater. Res. Bull. **12**, 251 (1977).
[12] K. J. D. MacKenzie, G. J. Gainford, and M. J. Ryan, J. Eur. Ceram. Soc. **16**, 553 (1996).
[13] P. L. Wang and P.-E. Werner, J. Mater. Sci. **32**, 1925 (1997).
[14] A. W. J. M. Rae, D. P. Thompson, N. J. Pipkin, and K. H. Jack, Spec. Ceram. **6**, 347 (1975).
[15] M. A. Sainz, P. Moranzo, and M. I. Osendi, J. Am. Ceram. Soc. **85**, 941 (2002).
[16] F. Peillon-Cluzel, F. Thevenot, and T. Epicier, Int. J. Refract. Met. Hard Mater. **19**, 419 (2001).
[17] I. Tanaka, S. Nasu, H. Adachi, Y. Miyamoto, and K. Niihara, Acta Metall. Mater. **40**, 1995 (1992).
[18] L'. Benco, J. Hafner, Z. Lencés, and P. Sajgalik, J. Am. Ceram. Soc. **86**, 1162 (2003).
[19] C. M. Fan and R. Metselaar, J. Am. Ceram. Soc. **86**, 1956 (2003).
[20] S. Hampshire, J. Non-Cryst. Solids **316**, 64 (2003).
[21] R. S. Aujla, G. Leng-Ward, M. H. Lewis, E. F. W. Seymour, G. W. West, and G. A. Styles, Philos. Mag. B **54** (2), L52 (1986).
[22] R. Dupree, M. H. Lewis, and M. E. Smith, J. Am. Chem. Soc. **110**, 1083 (1988).
[23] R. K. Harris, M. J. Leach, and D. P. Thompson, Chem. Mater. **1**, 336 (1989).
[24] A. Koroglu, D. C. Apperley, R. K. Harris, and D. P. Thompson, J. Mater. Chem. **6**, 1031 (1996).
[25] P.-L. Wang, P.-E. Werner, L. Gao, R. K. Harris, and D. P. Thompson, J. Mater. Chem. **7**, 2127 (1997).
[26] J. W. H. van Krevel, H. T. Hintzen, R. Metselaar, and A. Meijevink, J. Alloys Compd. **268**, 272 (1998).
[27] J. Carpena and J. L. Lacout, Brevet **93**, 08676 (1993).
[28] I. Tanaka, H.-J. Kleebe, M. K. Cinibulk, J. Bruley, D. R. Clarke, and M. Rühle, J. Am. Ceram. Soc. **77**, 911 (1994).
[29] C.-M. Wang, X. Pan, M. J. Hoffmann, R. M. Cannon, and M. Rühle, J. Am. Ceram. Soc. **79**, 788 (1996).
[30] X. Pan, H. Gu, R. van Weeren, S. C. Danforth, R. M. Cannon, and Manfred Rühle, J. Am. Ceram. Soc. **79**, 2313 (1996).
[31] H.-J. Kleebe, J. Ceram. Soc. Jpn. **105**, 453 (1997).
[32] Y.-M. Chiang, J.-R. Lee, and H. Wang, in *Ceramic Microstructure: Control at the Atomic Level*, edited by A. P. Tomsia and A. Glaeser (Plenum, New York, 1998), pp. 131–147.
[33] H. Gu, X. Pan, R. M. Cannon, and M. Rühle, J. Am. Ceram. Soc. **81**, 3125 (1998).
[34] R. M. Cannon, M. Rühle, M. J. Hoffmann, R. H. French, H. Gu, A. P. Tomsia, and E. Saiz, Ceram. Trans. **118**, 427 (2000).
[35] H. Gu, R. M. Cannon, H. J. Seifert, M. J. Hoffmann, and I. Tanaka, J. Am. Ceram. Soc. **85**, 25 (2002).
[36] H. Gu, T. Nagano, G. D. Zhan, M. Mitomo, and F. Wakai, J. Am. Ceram. Soc. **86**, 1753 (2003).
[37] E. Y. Sun, P. F. Becher, C.-H. Hsueh, G. S. Painter, S. B. Waters, S. L. Hwang, and M. J. Hoffmann, Acta Mater. **47**, 2777 (1999).
[38] P. F. Becher, G. S. Painter, E. Y. Sun, C. M. Hsueh, and M. J. Lance, Acta Mater. **48**, 4493 (2000).
[39] M. J. Hoffmann, in *Tailoring of Mechanical Properties of Si_3N_4 Ceramics*, edited by M. J. Hoffmann and G. Petzow (Kluwer Academic, Dordrecht, The Netherlands, 1994), pp. 59–72.
[40] D. R. Clark, J. Am. Ceram. Soc. **70**, 11 (1987).
[41] R. G. Horn, J. Am. Ceram. Soc. **73**, 11 (1990).
[42] D. R. Clark, T. M. Shaw, A. P. Philipse, and R. G. Horn, J. Am. Ceram. Soc. **76**, 1201 (1993).
[43] C. Wang, M. Mitomo, T. Nishimura, and R. Bando, J. Am. Ceram. Soc. **80**, 11 (1997).
[44] D. A. Litton and S. H. Garofalini, J. Am. Ceram. Soc. **83**, 2273 (2000).
[45] M. Yoshiya, I. Tanaka, and H. Adachi, Acta Mater. **48**, 4641 (2000).
[46] M. Yoshiya, K. Tatsumi, I. Tanaka, and H. Adachi, J. Am. Ceram. Soc. **85**, 109 (2002).
[47] X. Su and S. H. Garofalini, J. Mater. Res. **19**, 752 (2004).
[48] G. S. Painter, P. F. Becher, H.-J. Kleebe, and G. Pezzotti, Phys. Rev. B **65**, 064113 (2002).
[49] A. Ziegler, C. Kisielowski, M. J. Hoffmann, and R. O. Richie, J. Am. Ceram. Soc. **86**, 1777 (2003).
[50] Y.-N. Xu and W. Y. Ching, Phys. Rev. B **44**, 11 048 (1991).
[51] M.-Z. Huang, L. Ouyang, and W. Y. Ching, Phys. Rev. B **59**, 3540 (1999).
[52] Y.-N. Xu and W. Y. Ching, Phys. Rev. B **51**, 17 379 (1995).
[53] Y.-N. Xu, Z.-Q. Gu, and W. Y. Ching, Phys. Rev. B **56**, 14 993 (1997).
[54] W. Y. Ching, L. Ouyang, and Y.-N. Xu, Phys. Rev. B **67**, 245108 (2003).
[55] Lizhi Ouyang, Hongzhi Yao, Scott Richey, Y.-N. Xu, and W. Y. Ching, Phys. Rev. B **69**, 094112 (2004).
[56] W. Y. Ching, Y.-N. Xu, and L. Ouyang, J. Am. Ceram. Soc. **86**, 1424 (2003).
[57] P. D. E. Morgan (private communication).
[58] P. D. E. Morgan, J. Mater. Sci. **21**, 4305 (1986); J. Mater. Sci. Lett. **5**, 372 (1986).
[59] D. McKie and C. McKie, in *Crystalline Solids*, edited by T. Nelson (New York, 1974), pp. 324–426.
[60] C. M. Fang, G. A. deWijs, R. A. DeGroot, R. Metselaar, H. T. Hintzen, and G. deWith, Chem. Mater. **12**, 1168 (2000).
[61] H. T. Stokes and D. M. Hatch, ISOTROPY ⟨www.physics.byu.edu/~stokesh/isotropy.html⟩ (2002).
[62] W. Y. Ching, J. Am. Ceram. Soc. **73**, 3135 (1990).
[63] S. Saburi, A. Kawahara, C. Henmi, I. Kusachi, and K. Kihara, Mineral. J. **8**, 286 (1977).
[64] K. H. Jack, in *Nitrogen Ceramics*, edited by F. L. Riley (Noordhoff, Leyden, The Netherlands, 1977), p. 121.
[65] S. A. Kawahara, C. Henmi, I. Kusachi, and K. Kihara, Mineral. J. **8**, 286 (1977).
[66] M. A. Scott, D. L. Russell, B. Henderson, T. P. J. Han, and H. G. Gallagher, J. Cryst. Growth **183**, 366 (1998).
[67] See, *CRC Handbook of Bioactive Ceramics: Calcium Phosphate and Hydroxylapatite Ceramics*, edited by T. Yamamuro, L. L. Hench, and J. Wilson (CRC Press, New York, 1990), Vol. 2.
[68] B. D. Ratner, A. S. Hoffman, F. J. Schoen, and J. E. Lemon, *Biomaterials Science* (Academic, San Diego, CA, 1996).
[69] G. Kresse and J. Hafner, Phys. Rev. B **47**, 558 (1993).
[70] G. Kresse and J. Furthmuller, Comput. Mater. Sci. **6**, 15 (1996);

Phys. Rev. B **54**, 11 169 (1996).
[71] D. Vanderbilt, Phys. Rev. B **41**, 7892 (1990).
[72] G. Kresse and J. Hafner, J. Phys.: Condens. Matter **6**, 8245 (1994).
[73] R. S. Mulliken, J. Chem. Phys. **23**, 1833 (1955).
[74] Y.-N. Xu and W. Y. Ching, Phys. Rev. B **59**, 10 530 (1999).
[75] W. Y. Ching and Y.-N. Xu, Phys. Rev. B **59**, 12 815 (1999).
[76] Y.-N. Xu, W. Y. Ching, and B. K. Brickeen, Phys. Rev. B **61**, 1817 (2000).
[77] W. Y. Ching, Y.-N. Xu, and B. K. Brickeen, Phys. Rev. B **63**, 115101 (2001).
[78] L. Ouyang, Y.-N. Xu, and W. Y. Ching, Phys. Rev. B **65**, 113110 (2002).
[79] S.-D. Mo, L. Ouyang, W. Y. Ching, I. Tanaka, Y. Koyama, and R. Riedel, Phys. Rev. Lett. **83**, 24 (1999).
[80] W. Y. Ching, S.-D. Mo, L. Ouyang, I. Tanaka, and M. Yoshiya, Phys. Rev. B **61**, 10 609 (2000).
[81] W. Y. Ching, S.-D. Mo, I. Tanaka, and M. Yoshiya, Phys. Rev. B **63**, 064102 (2001).
[82] W. Y. Ching, S.-D. Mo, and L. Ouyang, Phys. Rev. B **63**, 245110 (2001).
[83] W. Y. Ching, S.-D. Mo, Y. Chen, P. Rulis, I. Tanaka, and M. Yoshiya, J. Am. Ceram. Soc. **85**, 75 (2002).
[84] W. Y. Ching, Yong-Nian Xu, and L. Ouyang, Phys. Rev. B **66**, 235106 (2002).
[85] L. Ouyang and W. Y. Ching, Appl. Phys. Lett. **81** 229 (2002).
[86] J. D. Brown, *The Chemical Bond in Inorganic Chemistry: Bond Valence Model* (Oxford University Press, Oxford, U.K., 2002).
[87] D. A. Muller, T. Sorsch, S. Moccio, F. H. Baumann, K. Evans-Lutterodt, and G. Timp, Nature (London) **399**, 758 (1999).
[88] M. L. Green, T. W. Sorsch, G. L. Timp, D. A. Muller, B. E. Weir, P. J. Silverman, S. V. Moccio, and Y. O. Kim, Microelectron. Eng. **48**, 25 (1999).
[89] G. D. Wilk and R. M. Wallace, Appl. Phys. Lett. **74**, 2854 (1999); *ibid.* **76**, 112 (2000).
[90] G. D. Wilk, R. M. Wallace, and J. M. Anthony, J. Appl. Phys. **87**, 484 (2000).
[91] E. M. Lizshitz, Sov. Phys. JETP **2**, 73 (1956).
[92] I. E. Dzyaloshinskii and E. M. Lizshitz, Sov. Phys. JETP **37**, 161 (1960).
[93] I. E. Dzyaloshinskii, E. M. Lizshitz, and L. P. Pitaevskii, Adv. Phys. **10**, 165 (1961).
[94] D. Tabor and R. H. S. Winterton, Proc. R. Soc. London, Ser. A **312**, 435 (1969).
[95] R. H. French, R. M. Cannon, L. K. DeNoyer, and Y.-M. Chiang, Solid State Ionics **75**, 13 (1995).
[96] R. H. French, J. Am. Ceram. Soc. **83**, 217 (2000).
[97] S.-D. Mo and W. Y. Ching, Phys. Rev. B **62**, 7901 (2000).
[98] S.-D. Mo, and W. Y. Ching, Appl. Phys. Lett. **78**, 3809 (2001).
[99] I. Tanaka, T. Mizoguchi, T. Sekine, H. He, K. Kimoto, S.-D. Mo, and W. Y. Ching, Appl. Phys. Lett. **78** 2134 (2001).
[100] Y.-N. Xu, Yu Chen, S.-D. Mo, and W. Y. Ching, Phys. Rev. B **65**, 235105 (2002).
[101] W. Y. Ching, S.-D. Mo, and Y. Chen, J. Am. Ceram. Soc. **85**, 11 (2002).
[102] S. J. Glass, F. M. Mahoney, B. Quillan, J. P. Pollinger, and R. E. Loehman, Acta Mater. **46**, 2393 (1998).